

Quark mass and chiral condensate from the Wilson twisted mass lattice quark propagator

Florian Burger^a, Vittorio Lubicz^{b,c}, Michael Müller-Preussker^a, Silvano Simula^{b,c},
Carsten Urbach^d



^a Humboldt-Universität zu Berlin, Institut für Physik, 12489 Berlin, Germany

^b Dip. di Fisica, Università Roma Tre, Via della Vasca Navale 84, I-00146 Roma, Italy

^c INFN, Sezione di Roma Tre, Via della Vasca Navale 84, I-00146 Roma, Italy

^d Universität Bonn, HISKP and Bethe Center for Theoretical Physics,
Nussallee 14-16, 53115 Bonn, Germany

October 2, 2012

Abstract

In this work, we report about the determination of nonperturbative OPE parameters from fits of continuum perturbation theory to the Landau gauge quark propagator. The propagators are computed numerically using lattice QCD with $N_f = 2$ dynamical Wilson twisted mass fermions. We use four different values of the lattice spacing ranging from $a \approx 0.1$ fm to $a \approx 0.05$ fm as well as several quark masses per lattice spacing. This allows us to obtain continuum results for the chiral condensate and the up/down quark mass extrapolated to the physical point. The main results are the average up/down quark mass $m_q^{\overline{\text{MS}}}(2 \text{ GeV}) = 3.0 (4) (2) \text{ MeV}$ at the physical point and $\langle \bar{\psi}\psi \rangle^{\overline{\text{MS}}}(2 \text{ GeV}) = -(299 (26) (29) \text{ MeV})^3$ in the chiral limit. We have also studied nonperturbative contaminations of our results at small values of the momenta, which are often interpreted as the contribution of the gluon condensate $\langle A^2 \rangle$. We do see contributions from such terms, which are, however, not stable over the order in perturbation theory.

PACS numbers: 11.15.Ha, 12.38.Ge, 12.38.Aw

Keywords: Lattice QCD, quark propagator, Landau gauge, condensates, quark mass

1 Introduction

Quantum Chromodynamics (QCD) describes the strong interaction part in our current standard model of elementary particle physics. Due to its particular properties, predictions for fundamental parameters of QCD require nonperturbative methods. The main tool in this context is lattice QCD, which allows predictions from first principles.

Also perturbative calculations in QCD, where applicable, play an important role for our understanding of QCD. For instance, in the regime of large momenta two-point functions $\langle O(p) O(p') \rangle$ of some operator $O(p)$ can be written in terms of an operator product expansion (OPE). The OPE contains coefficients carrying the dependence on the momenta, which can be computed in perturbation theory as asymptotic series in powers of the strong coupling α_s , multiplied with local operators and appropriate factors of the quark mass. The matrix elements of those local operators, like e.g. the chiral condensate, are of purely nonperturbative nature.

A most natural combination of the two aforementioned notions is to compute the momentum dependence of two point functions nonperturbatively and compare these for large momenta with the OPE prediction. Such a method not only allows us to compute estimates for fundamental parameters of QCD, such as quark masses and condensates, but in principle also to determine the strong coupling constant α_s .

The quantity we consider in this work is the Landau gauge quark propagator $P(k)$ in momentum space. Its OPE has the following form

$$P(k) \sim \frac{1}{k^2} (\not{k} C_1(k^2) + C_m(k^2) m_q + C_{\bar{\psi}\psi}(k^2) \langle \bar{\psi}\psi \rangle + \dots) . \quad (1)$$

The coefficient functions $C_X(k^2)$, $X \equiv 1, m, \bar{\psi}\psi, \dots$ carry the whole momentum dependence and can be computed in perturbative QCD for large k^2 . The nonperturbative information is encoded in the quark mass and the condensate(s).

Since we are going to compute $P(k)$ using lattice QCD, we cannot perform the calculation at arbitrary values for the momenta, since we have to fulfil the inequality

$$1/a^2 \gtrsim k^2 \gtrsim \Lambda_{\text{QCD}}^2 .$$

The first inequality ensures small lattice artifacts and the second one the applicability of perturbation theory. It is not a priori clear that such a window exists and one of the questions we try to answer in this work is whether the values of the lattice spacing available from state of the art lattice QCD simulations are yet sufficient for such an investigation. Hence, we will pay special attention to both, lattice artifacts and nonperturbative contaminations of our results.

Lattice artifacts have actually previously been a complication for the applicability of the method we are going to apply: when Wilson fermions are used naively in momentum space the leading contribution to the OPE of the quark propagator is a constant term proportional to the lattice spacing a . Even though this term will vanish eventually in the continuum limit, at finite value of a it will dominate the OPE, since the mass and condensate contributions are suppressed by powers of $1/k^2$. This makes the determination

of the chiral condensate difficult, whereas the quark mass can be determined if several values of it are investigated [1]. This complication can be circumvented by using the OPE of the pseudo-scalar vertex [2] or by working in the x -space [3].

Within the lattice formulation we are going to use here – the so-called Wilson twisted mass formulation of lattice QCD [4] – such a term can be avoided due to automatic $\mathcal{O}(a)$ improvement [5]. In addition, we are going to remove lattice artifacts of order $g_0^2 a^2$ from our data as computed in one-loop lattice perturbation theory [6, 7].

The procedure outlined above is not the only way to determine the quark mass and the chiral condensate. They have been determined previously for instance from fits of chiral perturbation theory to the data for the pseudoscalar decay constant and mass, see for instance [8]. But the analysis we are going to apply represents an independent way to determine these important standard model parameters with different systematics compared to other methods.

The main results of this paper are determinations of the average up/down quark mass at the physical point and of the quark condensate, both within the $\overline{\text{MS}}$ scheme at renormalization scale 2 GeV¹

$$m_q^{\overline{\text{MS}}}(2 \text{ GeV}) = 3.0 (4) (2) \text{ MeV} \quad (2)$$

and having performed the chiral limit

$$\langle \bar{\psi}\psi \rangle^{\overline{\text{MS}}}(2 \text{ GeV}) = -(299 (26) (29) \text{ MeV})^3. \quad (3)$$

For the chiral condensate we quote here the value stemming from one of our fit strategies (fit B), as explained later. The other fit strategies give slightly different, but compatible results. We also discuss nonperturbative contaminations at small momenta, called two-dimensional gluon condensate $\langle A^2 \rangle$ and provide effective values for it depending on the order of perturbation theory taken into account in the fits.

The investigation presented in this paper is based on gauge configurations as produced by the European Twisted Mass collaboration (ETMC) with $N_f = 2$ quark flavors of Wilson twisted mass fermions [8, 9, 10, 11]. We refer the reader to these references for all the details of the simulations.

The paper is organized as follows. In Sec. 2 we discuss the quark propagator in perturbation theory and in Sec. 3 our lattice formulation. In Sec. 4 we present our analysis strategy and in Sec. 5 the corresponding results. We conclude with a summary.

2 The Quark Propagator in Perturbation Theory

In perturbation theory the quark propagator is known up to three loops [12]. Recently, the OPE of the renormalized momentum space quark propagator in Landau gauge has been performed in Ref. [13] in the $\overline{\text{MS}}$ scheme. The authors have included terms up to mass dimension three in their calculations. According to its Lorentz structure, $P(k)$ can

¹The first errors are purely statistical and the second ones systematic, respectively.

be written as

$$P(k) = \frac{1}{k^2} S(k^2) \mathbf{1} + \frac{k}{k^2} V(k^2). \quad (4)$$

Assuming that we can use the OPE, one gets the following expansion for the scalar and vector form factors $S(k^2)$ and $V(k^2)$ [13] (up to operators of dimension three):

$$\begin{aligned} \frac{1}{k^2} S(k^2) &= C_m(k^2) m_q + \frac{C_{m^3}(k^2)}{k^2} m_q^3 + \\ &+ \frac{C_{mA^2}(k^2)}{k^2} m_q \langle A^2 \rangle + \frac{C_{\bar{\psi}\psi}(k^2)}{k^2} \langle \bar{\psi}\psi \rangle \end{aligned} \quad (5)$$

and

$$\frac{1}{k^2} V(k^2) = C_1(k^2) \mathbf{1} + \frac{C_{m^2}(k^2)}{k^2} m_q^2 + \frac{C_{A^2}(k^2)}{k^2} \langle A^2 \rangle. \quad (6)$$

While the quark mass m_q and the chiral condensate $\langle \bar{\psi}\psi \rangle$ are clearly of physical origin, the existence of a gluon condensate $\langle A^2 \rangle$ is debatable. However, in the OPE such a term is not excluded. The Wilson coefficients C_1 , C_m , C_{A^2} , C_{m^2} , $C_{\bar{\psi}\psi}$, C_{mA^2} and C_{m^3} are functions of the strong coupling constant $\alpha_s(\mu)$. The expansion can be found in Ref. [13]. The value of $\alpha_s(\mu)$ can be computed via renormalization group (RG) evolution as described in Ref. [14], which needs $\Lambda_{\overline{\text{MS}}}$ as an input. For this purpose we use a literature value, as discussed later on.

Although known up to a certain order in α_s , the perturbative series of the Wilson coefficients in Eqs. (5) and (6) may be truncated further in order to study the systematic effect of the truncation. For this purpose we stop the evaluation of the perturbative series at the n_{max} 'th power in α_s including at maximum terms of order $\alpha_s^{n_{\text{max}}}$:

$$C_X = C_X^0 + C_X^1 \alpha_s^1 + \dots + C_X^{n_{\text{max}}} \alpha_s^{n_{\text{max}}}, \quad (7)$$

where X stands for 1 , A^2 , m^2 , \dots . The truncation is consistently done in the Wilson coefficients as well as in the evolution of α_s by means of the β -function.

3 Lattice Formulation

The lattice quark propagator is calculated within the twisted mass formulation of $N_f = 2$ QCD [8, 9, 10, 11]. For a review see Ref. [15]. The gauge action used to generate the ensembles was the tree level Symanzik improved gauge action (tlSym) [16], viz.

$$S_g = \frac{\beta}{3} \sum_x \left(b_0 \sum_{\substack{\mu, \nu=1 \\ 1 \leq \mu < \nu}}^4 \{1 - \text{ReTr} (U_{x, \mu, \nu}^{1 \times 1})\} + b_1 \sum_{\substack{\mu, \nu=1 \\ \mu \neq \nu}}^4 \{1 - \text{ReTr} (U_{x, \mu, \nu}^{1 \times 2})\} \right),$$

with the bare inverse gauge coupling $\beta = 6/g_0^2$, $b_1 = -1/12$ and $b_0 = 1 - 8b_1$. The fermion action in the so-called twisted basis is given by:

$$S_F = a^4 \sum_x \bar{\chi}_x (D_W + m_0 + i\mu_q \gamma_5 \tau_3) \chi_x \equiv a^4 \sum_x \bar{\chi}_x D_{\text{tm}} \chi_x. \quad (8)$$

Here D_W represents the lattice Wilson Dirac operator, m_0 is the usual bare quark mass and μ_q is the bare twisted quark mass, which is multiplied by the third Pauli matrix τ_3 acting in flavor space. Twisted mass fermions are said to be at *maximal twist* if the bare untwisted quark mass m_0 is tuned to its critical value m_{crit} , the situation we are working in. At maximal twist, the twisted quark mass μ_q is related directly to the physical quark mass and renormalizes multiplicatively only. Many mixings under renormalization are expected to be simplified [5, 17]. And – most importantly – as was first shown in Ref. [5], physical observables are automatically $\mathcal{O}(a)$ improved without the need to determine any operator-specific improvement coefficients. For details on tuning to maximal twist we refer the reader to Ref. [8]. The aforementioned twisted basis $\bar{\chi}, \chi$ is at maximal twist related to the standard physical basis $\bar{\psi}, \psi$ via the axial chiral rotation

$$\psi = e^{i\pi\gamma_5\tau_3/4} \chi, \quad \bar{\psi} = \bar{\chi} e^{i\pi\gamma_5\tau_3/4}. \quad (9)$$

In this framework we compute the Landau gauge twisted quark propagator $P_{\text{tm}}(x)$ in position space

$$P_{\text{tm}}(x) = \langle \chi_x \bar{\chi}_0 \rangle = \langle (D_{\text{tm}})^{-1} \rangle_U, \quad (10)$$

where $\langle \dots \rangle_U$ denotes the average over gauge field configurations $\{U\}$ collected by the ETMC, which were gauge fixed to Landau gauge using the overrelaxation method described in [18].² The quark propagators calculated on these configurations are Fourier transformed to momentum space and then rotated into the physical basis using Eq. (9) yielding

$$P(k) = \frac{1}{\sqrt{2}} (\mathbb{1} + i\gamma_5\tau^3) P_{\text{tm}}(k) \frac{1}{\sqrt{2}} (\mathbb{1} + i\gamma_5\tau^3). \quad (11)$$

The details of the ETMC ensembles we used can be found in Table 1. In total we consider four values of the inverse gauge coupling β corresponding to values of the lattice spacing ranging from 0.1 fm to about 0.051 fm [8], with a statistics of 240 gauge configurations for most of the ensembles considered. The values of the (charged) pseudoscalar mass range from 600 MeV down to 250 MeV. For setting the scale we use the results published by ETMC in Ref. [8].

On the lattice, Eq. (4) is valid only up to lattice artifacts. In particular, since parity is not a good symmetry of Wilson twisted mass fermions at finite values of the lattice spacing, a parity violating term in the propagator is allowed, which is formally $\mathcal{O}(a)$. Ignoring higher order lattice artifacts including $O(4)$ symmetry breaking terms, the lattice quark propagator can be written as follows [20]

$$P(k) = -i \frac{\not{k}}{k^2} V(k^2) + \frac{1}{k^2} S(k^2) + i\gamma_5\tau^3 \frac{1}{k^2} G(k^2). \quad (12)$$

The parity violating term $G(k^2)$ comes with opposite sign for up and down propagators. Averaging over up and down propagators hence eliminates these artifacts [20]. Note that

²Gribov copy effects have been found to be small for large momenta in studies of the lattice gluon and ghost propagators in Ref. [19]. We have also carried out a study on the Gribov copy dependence of the quark propagator on a test ensemble with smaller lattice size and have found no ambiguities there.

Ensemble	β	$L^3 \times T$	$a\mu_q$	a [fm]	N_{conf}
A_1	3.80	$24^3 \times 48$	0.0060	≈ 0.10	231
A_2			0.0080		240
A_3			0.0110		240
A_4			0.0165		240
B_1	3.90	$24^3 \times 48$	0.0040	≈ 0.085	240
B_2			0.0064		240
B_3			0.0085		240
B_4			0.0100		240
B_5			0.0150		240
C_1	4.05	$32^3 \times 64$	0.0030	≈ 0.067	240
C_2			0.0060		161
C_3			0.0080		163
D_1	4.20	$48^3 \times 96$	0.0020	≈ 0.051	188
D_2		$32^3 \times 64$	0.0065		200

Table 1: Details of the ETMC gauge ensembles, used in the analysis. See Ref. [8] for more details.

the parity violating $\mathcal{O}(a)$ term encoded in $G(k^2)$ contributes to $S(k^2)$ for standard Wilson fermions.

Rotational symmetry is broken at finite values of the lattice spacing. In order to reduce the impact of those artifacts on our results, we carried out the following steps: firstly, we use for the analysis the lattice tree level momenta of the quark propagator, $k_\mu = \frac{1}{a} \sin(a\tilde{k}_\mu + \frac{1}{2}\delta_{\mu 0})$ with $\tilde{k}_\mu = (2\pi n_\mu)/(aL_\mu)$. Secondly, we restrict ourselves to momenta lying near the lattice diagonal (i. e. off-axis) by applying the so-called cylinder cut [21]

$$\left(\sum_{\mu} \left(\frac{n_{\mu}}{L_{\mu}} \right)^2 \right) - \left(\sum_{\mu} \left(\frac{n_{\mu} \hat{N}_{\mu}}{L_{\mu}} \right) \right)^2 \leq \frac{C_{\text{cyl}}}{L^2}, \quad (13)$$

where $\hat{N}_{\mu} = 0.5 \cdot (1, 1, 1, 1)$ is the lattice diagonal. The constant has been set to $C_{\text{cyl}} = 1.6$ for the large lattice at $\beta = 4.2$ and to $C_{\text{cyl}} = 1.1$ elsewhere. Following this procedure, the data for $S(k^2)$ and $V(k^2)$ show a sufficiently smooth behavior.

Finally, we correct the form factors for lattice artifacts of order $\mathcal{O}(g_0^2 a^2)$. These corrections have been computed explicitly in Ref. [6, 7] within one-loop lattice perturbation theory.

4 Analysis

The basic quantities considered in our analysis are the bare form factors $V(k^2)$ and $S(k^2)$ of the lattice quark propagator Eq. (12) after applying the cylinder cut and after removing lattice artifacts of the order $\mathcal{O}(g_0^2 a^2)$. We shall denote these *corrected* form factors with \hat{S} and \hat{V} . The $\mathcal{O}(g_0^2 a^2)$ artifacts have only modest effect on the ratio S/V (after performing

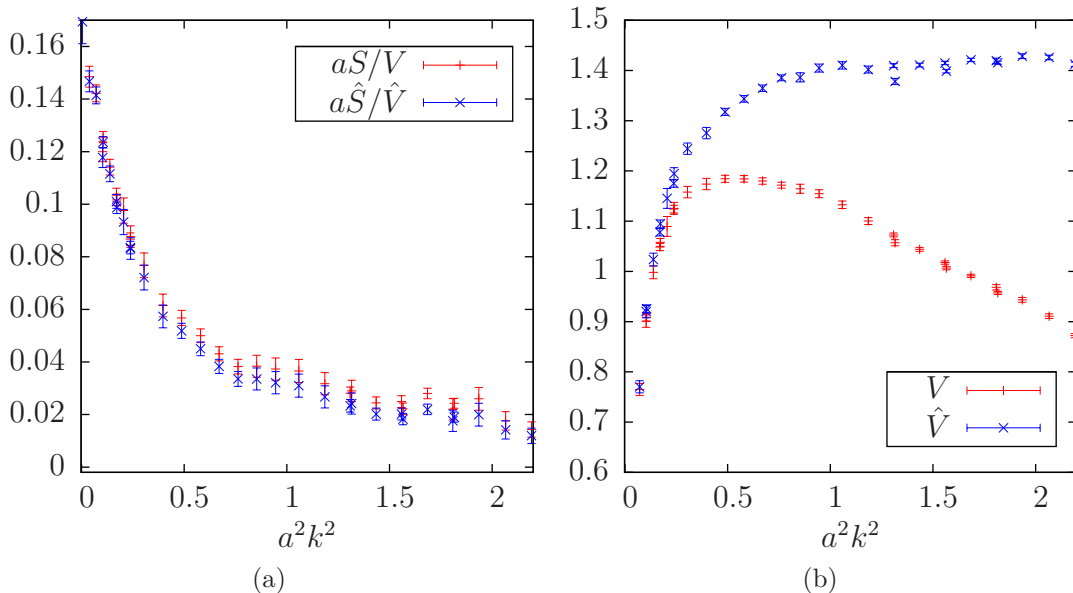


Figure 1: Effect of the correction for $\mathcal{O}(g_0^2 a^2)$ artifacts on S/V (left) and on V (right) for $\beta = 3.8$. The effect becomes weaker for larger β as expected.

the cylinder cut) while V alone receives substantial corrections. As an example we show in Fig. 1 uncorrected and corrected data for aS/V and V for $\beta = 3.8$ in the left and right panel, respectively. At this (smallest) β -value one sees dramatic corrections to V . However, as visible in Fig. 2, the corrections decrease as the continuum limit is approached. Our goal is to determine the renormalized quark mass and the chiral condensate. Looking at the OPE's Eqs. (5) and (6) it seems appropriate to study $\hat{S}(k^2)$, since the quark mass can be determined from its leading quark mass dependence and the chiral condensate is the leading contribution in the chiral limit. However, if one wants to avoid the usage of renormalization constants, it appears to be useful to consider the scalar-to-vector form factor ratio

$$\hat{R}(k^2) \equiv \frac{\hat{S}(k^2)}{\hat{V}(k^2)}, \quad (14)$$

since the renormalization constant cancels out. \hat{S} and \hat{V} are then replaced by their perturbative series and the resulting expression is fitted to our numerical data for $\hat{R}(k^2)$ with the renormalized quark mass, the renormalized chiral condensate and possibly further terms as fit parameters. We remark in passing that as soon as the renormalization constants in \hat{R} cancel in between nominator and denominator, the OPE of \hat{R} is written in renormalized quantities only. Scheme and renormalization scale depend then on the scheme and scale the perturbative expansion is performed in.

For the fits of the ratio \hat{R} as well as of the formfactors \hat{S} and \hat{V} separately we have followed three different strategies.

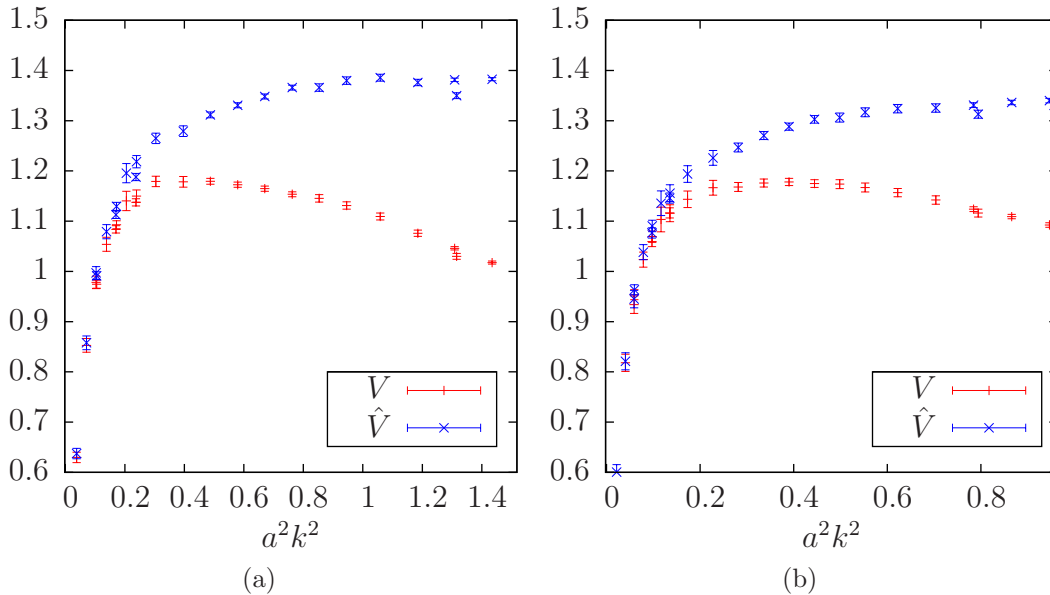


Figure 2: Same as in Fig. 1(b) but for $\beta = 3.9$ (left) and $\beta = 4.05$ (right). The x -axis always displays the same physical momentum range such that these figures may be compared.

1. Fit A:

The fits of Eq. (14) to the data are performed simultaneously to all ensembles at fixed β -values, allowing for a different fit parameter value m_q for each ensemble, but only for one global fit parameter corresponding to $\langle \bar{\psi}\psi \rangle$. All other contributions from the OPE are neglected. At each value of β the results for m_q are then interpolated to reference values of $r_0 m_{\text{PS}}$, r_0 denoting the so-called Sommer scale [22] and m_{PS} the pseudo-scalar meson mass, respectively. Those interpolated results are extrapolated to the continuum limit and then to the physical point where appropriate.

2. Fit B:

Resigning to determine a value for the renormalized quark mass, we extrapolate our data for $\hat{R}(k^2)$ to the chiral limit at each β -value first. Only then we fit the perturbative series to the data at each β -value, with terms proportional to powers of m_q set to zero and still neglecting all other contributions from the OPE. Thereafter the result for $\langle \bar{\psi}\psi \rangle$ is extrapolated to the continuum limit.

3. Fits A' and B' :

At small values of k^2 our data is potentially contaminated by additional nonperturbative terms in the OPE. One example is what is often called the gluon condensate $\langle A^2 \rangle$. We shall avoid here the discussion of its mere existence (see also [23, 24, 25]), but we shall investigate whether our data is contaminated by effects that may effectively look like the gluon condensate. Since including such a term into the fits of type A or B applied to the ratio \hat{R} appears to be not stable, we first determine

$\langle A^2 \rangle$ from $\hat{V}(k^2)$ only, and use it afterwards as an input for a fit of type A and B .

4. Fit C :

As a further check of the sensitivity of the extraction of the quark and gluon condensates against different assumptions in the fitting procedures, we resign to determine the quark masses m_q (as in fits B and B') and instead we fix their values to the ones of the renormalized quark masses, which at maximal twist are given by the twisted bare quark masses, $a\mu_q$, multiplied by $1/Z_P$, where Z_P is the renormalization constant of the pseudoscalar current³. In what follows, we will refer to such values as the Z_P -based quark masses.

Contrary to the previous fits A and B , we do not use the data for the ratio given by Eq. (14), but instead the data for the two form factors, \hat{S} and \hat{V} , separately in order to improve the sensitivity to the value of the gluon condensate, and moreover we consider simultaneously all the data for the four values of the lattice spacing. To this end we have to consider explicitly the values of the renormalization constant of the quark field, Z_q , which will be treated as free parameters, and we introduce also simple discretization terms, proportional to the square of the lattice spacing, for the quark masses and the condensates (see next section).

We perform fully correlated fits using the inverse covariance matrix in our χ^2 -functions as described in Ref. [27]. In order to estimate the systematic error induced by a specific choice of the fit range we have performed all fits in several fit ranges. The results we give are then weighted according to the χ^2 -distribution function and our final result consists of the weighted average over all fit ranges [8]. The fit ranges are consistently chosen among different values of the lattice spacings in such a way that the physical momentum range in terms of $r_0^2 k^2$ is kept approximately constant. The different sets of fit ranges we used are

$$\begin{aligned} r_0^2 k^2 \in & [18, \dots, 58], [18, \dots, 64], [18, \dots, 66], \\ & [19, \dots, 64], [20, \dots, 64], [21, \dots, 64], \end{aligned} \quad (15)$$

which in physical units lie within the range

$$3.9 \text{ GeV}^2 \leq k^2 \leq 14.6 \text{ GeV}^2. \quad (16)$$

The statistical errors are estimated using a bootstrap procedure to propagate the errors consistently to the next step of the analysis. In order to estimate the systematic error related to the truncation in the perturbative series we carried out the fits using $n_{\text{max}} = 2$ and $n_{\text{max}} = 3$ and we take the difference in the results as systematic uncertainty.

The evaluation of the perturbative series requires a value of α_s as input, for which a value of $\Lambda_{\overline{\text{MS}}}$ is needed. For this purpose we use the value $\Lambda_{\overline{\text{MS}}} = 0.330(23) \text{ GeV}$ [24] (see also Table 2) which is in good agreement with other $N_f = 2$ determinations of the same quantity [28, 29]. The error of this number is taken into account in our bootstrap analysis and contributes to the statistical errors of our fit results.

³The values of Z_P in the $\overline{\text{MS}}$ scheme at a renormalization scale of 2 GeV can be read off from Ref. [20] at $\beta = 3.80, 3.90, 4.05$ and from Ref. [26] at $\beta = 4.20$.

m_{π^0} [MeV]	r_0 [fm]	$\Lambda_{\overline{\text{MS}}}$ [GeV]
134.9766(6)	0.42(2)	0.330(23)

Table 2: Physical quantities used as an input parameters for the fits and analysis. The values of m_{π^0} and r_0 have been taken from Refs. [30, 8]. The value of $\Lambda_{\overline{\text{MS}}}$ is taken from Ref. [24].

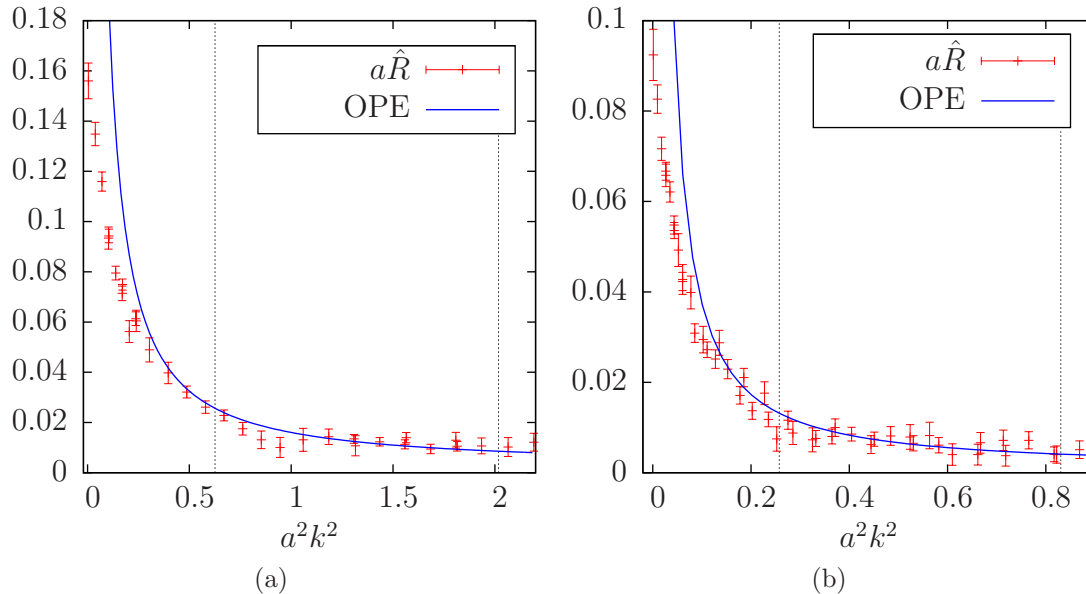


Figure 3: Fits of \hat{R} in lattice units to our data for ensemble B_1 at $\beta = 3.9$ (left) and ensemble D_1 at $\beta = 4.2$ (right). The vertical lines indicate the fit range. These plots correspond to fit strategy A.

5 Results

5.1 Fit A: Determination of Quark Condensate and Mass

Ignoring terms proportional to $\langle A^2 \rangle$ and higher order terms in the OPE Eqs. (5) and (6), we have performed fits to the chirally non-extrapolated data of \hat{S}/\hat{V} with the quark mass and the chiral condensate as fit parameters only. The fits are performed as discussed previously. Throughout this analysis the renormalization scale has been fixed at $\mu = 2$ GeV in the perturbative series.

For all fit ranges quoted above the fits have produced stable results with acceptable χ^2/dof values ranging from 0.78 to 1.24. We could not increase the lower boundary beyond $r_0^2k^2 = 21$ as the fit for $\beta = 3.8$ then turned unstable. In all considered fit ranges the fitted values of the quark mass and the chiral condensate have been compatible with each other within errors.

In Figs. 3(a) and 3(b) we show exemplary fits for ensemble B_1 at $\beta = 3.9$ and D_1 at $\beta = 4.2$ with dashed vertical lines indicating the chosen fit range.

In order to perform a continuum extrapolation of the fitted quark masses m_q we first have to interpolate (extrapolate) the values to common reference points of the squared pseudoscalar mass m_{PS}^2 at each β -value. We have chosen the following reference points

$$r_0^2 m_{\text{PS}}^2 \in \{0.49, 0.81, 1.21, 1.60\},$$

which allow us to use interpolations in the pseudoscalar mass in most of the cases. Only for $\beta = 4.05$ and $\beta = 4.2$ we have to perform a short extrapolation for the largest reference mass $r_0^2 m_{\text{PS}}^2 = 1.60$ and for $\beta = 3.8$ and $\beta = 3.9$ we have to rely on extrapolations for the smallest reference point. In Fig. 4 we show as an example the interpolation to these reference points for $\beta = 3.9$ and $\beta = 4.2$.

For each reference point we perform a separate continuum limit of the quantity $r_0 m_q$ in a^2 which is shown in Fig. 5(a). The data appears to be compatible with a linear behavior in a^2 for all chosen reference points as expected.

Finally, the continuum quark mass data has to be extrapolated to the physical pion mass $m_{\pi^0} = 134.9766$ (6) MeV [30], for which we use a linear curve with zero intercept (leaving the intercept free gives compatible results). The extrapolation is shown in Fig. 5(b). For $\langle \bar{\psi}\psi \rangle$ we have also performed a continuum extrapolation linear in a^2 as shown in Fig. 6. Note that we also tried to include chiral logs for the quark mass dependence of m_{PS}^2 , however, at our current precision this does not make a difference.

After performing a weighted average over the chosen fit ranges we quote the following results for Fit A:

$$\frac{\langle \bar{\psi}\psi \rangle^{\overline{\text{MS}}}}{N_f}(2 \text{ GeV}) = -(335 \text{ (37) (35) MeV})^3, \quad m_q^{\overline{\text{MS}}}(2 \text{ GeV}) = 3.0 \text{ (4) (2) MeV}, \quad (17)$$

where the first error is statistical and the second is a systematic error reflecting the uncertainties related to the fit range and to the truncation of the perturbative series. The systematic error due to the variation of the fit range is taken as the maximum deviation from the χ^2 -averaged result. This amounts to about 0.08 MeV $((5 \text{ MeV})^3)$ systematic uncertainty for the quark mass (condensate). Furthermore, decreasing the perturbative order to $n_{\text{max}} = 2$ results in a smaller fitted quark mass value as well as a higher value for $\langle \bar{\psi}\psi \rangle$. The systematic errors we quote is the change of the central values when we apply this modification and added by the change caused by varying the fit range.

5.2 Fit B: Determination of $\langle \bar{\psi}\psi \rangle$ in the Chiral Limit

As in the chiral limit the chiral condensate is the only nonperturbative parameter (disregarding again a possible gluon condensate) we expect it to be estimated more reliably and with less statistical error than in the finite mass case. Having calculated the quark propagator for two to five bare twisted quark mass values μ_q we can perform a chiral extrapolation for each lattice spacing separately. This limit has been performed linearly in the bare twisted quark mass $a\mu_q$ for $\hat{R}(k^2)$. Fig. 7(a) shows exemplary fits for $\beta = 3.9$ at three representative values of $a^2 k^2$, one at the lower end, one in the middle and one at

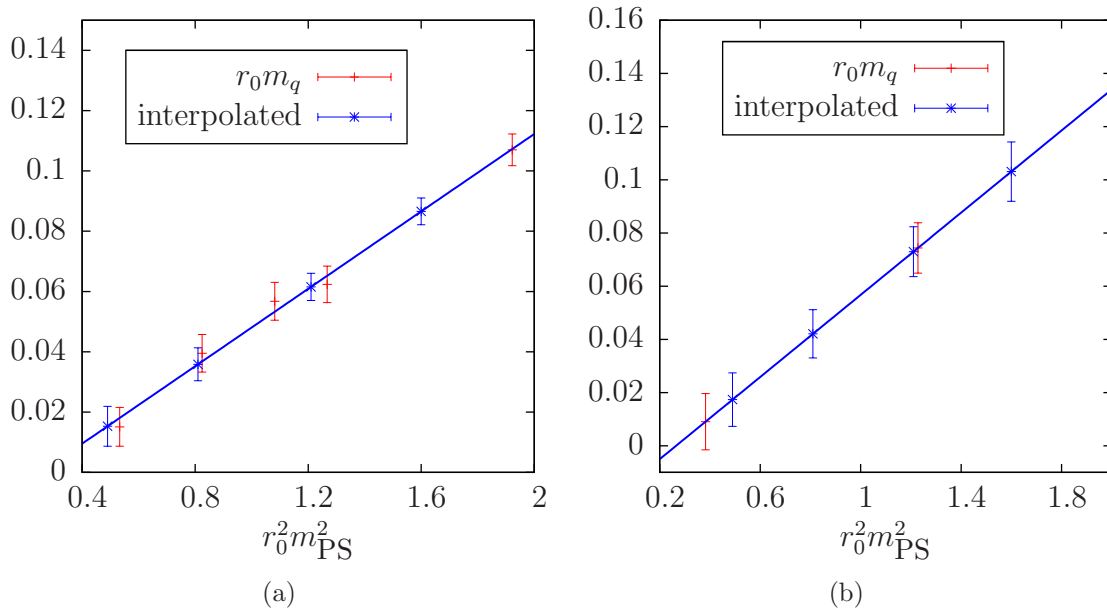


Figure 4: Interpolation to the four chosen pion mass reference points in m_{PS}^2 for $\beta = 3.9$ (left) and $\beta = 4.2$ (right). We also show the linear fit used for interpolation to the reference points. The blue points correspond to the interpolated values. These plots correspond to strategy fit A.

the upper end of the considered momentum range. For any lattice spacing and any other momentum not shown here the data is consistent with such an extrapolation.

We have then fitted the mass extrapolated data via Eqs. (5) and (6) disregarding all other OPE terms. The corresponding one parameter fits in $\langle\bar{\psi}\psi\rangle$ have produced χ^2/dof values in the range 0.8 to 1.8 and have been performed in the fit ranges:

$$r_0^2 k^2 \in [7, \dots, 64], [9, \dots, 64], [12, \dots, 64], [7, \dots, 60], [7, \dots, 58], [7, \dots, 56]. \quad (18)$$

Note that we had to extend the fit range compared to fit A towards the infrared in order to be sensitive to the curvature of the chirally extrapolated data and to obtain stable results. As an example we show the fit for $\beta = 4.05$ in Fig. 8(a). The continuum extrapolation has again been performed in the lattice spacing squared and is shown in Fig. 8(b). After a weighted average over the different fit ranges and the continuum extrapolation we get the following result for the chiral condensate:

$$\frac{\langle\bar{\psi}\psi\rangle^{\overline{\text{MS}}}}{N_f}(2 \text{ GeV}) = -(299 (26) (29) \text{ MeV})^3, \quad (19)$$

where again the second error is systematic. Lowering the perturbative order to $n_{\text{max}} = 2$ results in a higher value of $\langle\bar{\psi}\psi\rangle$. The systematic error due to the use of different fit ranges is evaluated in the same manner as for fit A and amounts to $(6 \text{ MeV})^3$.

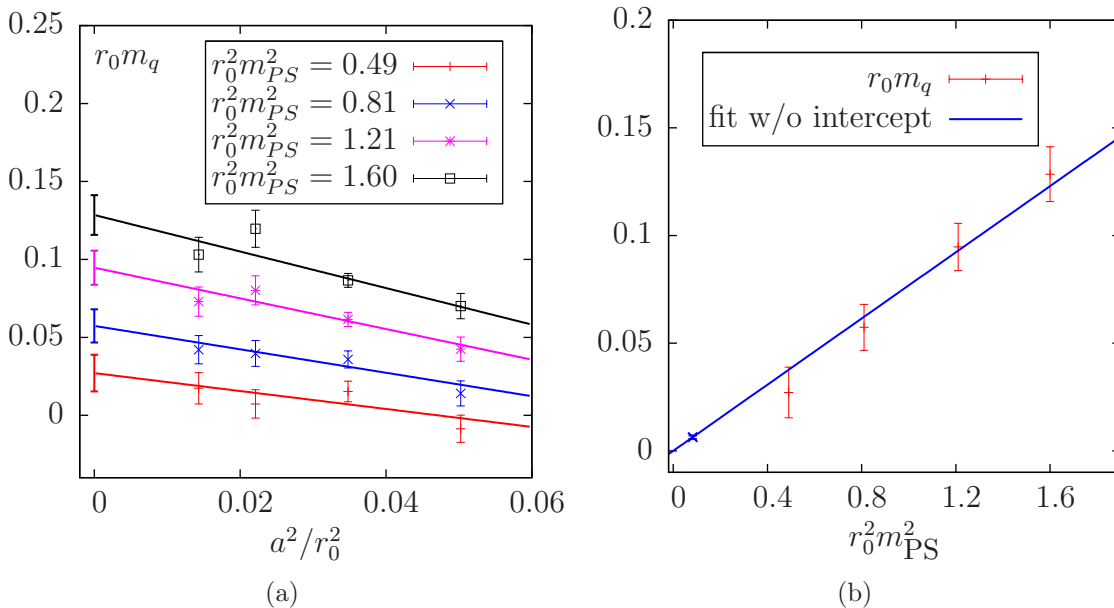


Figure 5: Continuum limit of $r_0 m_q$ for the four chosen reference points (left) and extrapolation of the continuum extrapolated quark mass values $r_0 m_q$ to the physical pseudoscalar mass (right). The linear fit has been constrained to go through the origin. This result again corresponds to fit A.

5.3 Fits A' and B' : Nonperturbative A^2 Contamination

As discussed in the introduction, on the lattice we have to restrict the analysis of the quark propagator to a window in the squared momenta, as for too small momenta the perturbative expansion will not be valid and for too large momenta lattice artifacts will be too large. Of course, with any choice of this window one can never be sure to be free of this sort of artifacts. For this reason we extend our analysis by including the further terms $m\langle A^2 \rangle$ and $\langle A^2 \rangle$ in the OPE. Unfortunately, it turns out that an inclusion of these terms as fit parameters in the fit to our data for $\hat{R}(k^2)$ appears to be not stable. This is why we follow a different strategy: we first determine an estimate for $\langle A^2 \rangle$ from $\hat{V}(k^2)$ in the chiral limit alone, and use this estimate to repeat the fits we discussed before. This is not a fully consistent treatment, but it should provide an estimate of the uncertainty in our results.

In more detail, we first studied $\hat{V}(k^2)$ of the quark propagator according to Eq. (6) in the chiral limit. In this form factor the dimension two term represents the first non-perturbative OPE contribution when the quark mass is extrapolated to zero and thus one has a direct handle on this term. A similar study has been done using the inverse lattice quark propagator in Ref. [31]. Note that unlike $\hat{R}(k^2)$ the form factor \hat{V} requires renormalization, which we include as free parameters into our fits.

The chiral limit of $\hat{V}(k^2)$ has been performed constant in $a\mu_q$. This is justified as can

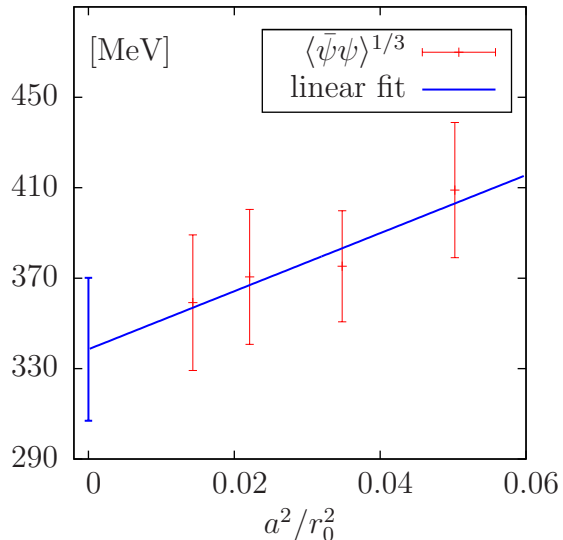


Figure 6: Continuum limit of $\langle \bar{\psi}\psi \rangle$ from fit A.

be seen for instance in Fig. 7(b) where we show the chiral limit of \hat{V} for $\beta = 3.90$ for three values of a^2k^2 . We then fit the OPE formula, Eq. (6), to our data for $\hat{V}(k^2)$ in the same fit ranges as used for the fits A and B. We obtain rather large values for χ^2/dof of about $\approx 5 - 7$ for $\beta = 3.8$ and $\beta = 3.9$ which are related to the fact that the cut in momenta we have applied does not work well for two points of \hat{V} at $a^2k^2 \approx 1.3$ and $a^2k^2 \approx 1.55$ (see the slight spread of the data at these regions in Fig. 1(b)). If we had discarded these points we would have obtained $\chi^2/\text{dof} < 3.5$ in both cases. The fits for the two smallest lattice spacings has yielded acceptable values of χ^2/dof staying below $\approx 1.3(1.5)$ for $\beta = 4.05(4.2)$ (see Fig. 9(a)). Finally, the results have been extrapolated to the continuum limit linearly in a^2 , as shown in Fig. 9(b). For the gluon condensate in the continuum limit we obtain

$$\langle A^2 \rangle^{\overline{\text{MS}}} = 0.65 (09) (17) \text{ GeV}^2.$$

The large systematic error is dominated by the truncation of the perturbative order. In order to better understand the role of the $\langle A^2 \rangle$ term in the OPE, we have studied the dependence of the values of $\langle A^2 \rangle$ on the order of perturbation theory that has been used in Eq. (6). To this end we have truncated perturbation theory at the order $\alpha_s^{n_{\text{max}}}$ and have performed fits with n_{max} ranging from 1 to 3. For these fits we have restricted ourselves to only one fit range with $9 \leq r_0^2 k^2 \leq 64$. The resulting values of $\langle A^2 \rangle$ have then been extrapolated linearly in a^2/r_0^2 to the continuum, as shown in Fig. 9(b) for $n_{\text{max}} = 2$.

In Fig. 10 we show the continuum extrapolated expectation value of $\langle A^2 \rangle$ as a function of n_{max} . From the figure we conclude that with increasing n_{max} the continuum value of $\langle A^2 \rangle$ decreases with no saturation visible (yet). Hence, we might conclude that this dimension two term is effectively describing higher order terms in perturbation theory which are not included in our analysis, see Ref. [32] for a discussion. However, it seems

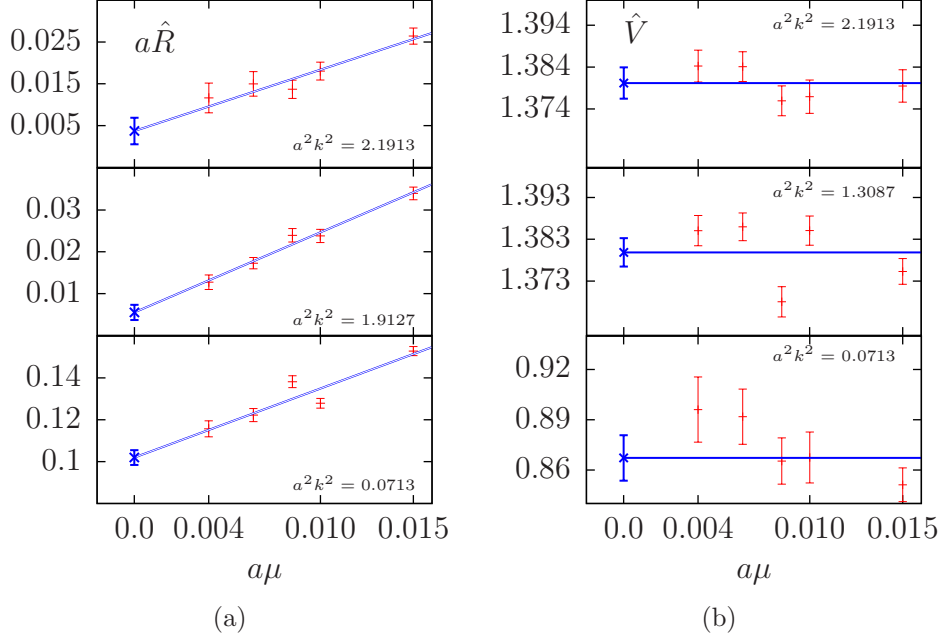


Figure 7: (left) Chiral limit for \hat{R} at $\beta = 3.9$. Data has been extrapolated assuming a linear dependence on the bare quark mass $a\mu_q$ which is compatible with our data at every momentum considered. (right) Chiral limit for \hat{V} at $\beta = 3.9$ assuming a constant dependence on the bare quark mass $a\mu_q$. Here we follow fit strategy *B*.

that this contamination is not negligible for our data when momenta as low as $r_0^2 k^2 \sim 9$ ($k^2 \sim 2 \text{ GeV}^2$) are included in the fit.

Next we investigate the influence of this $\langle A^2 \rangle$ term on the results for $\langle \bar{\psi}\psi \rangle$ and the quark mass. To this end we use the values of $\langle A^2 \rangle$ determined as discussed above as an input for fit with strategies *A* and *B* with fit ranges given in Eq. (15) and Eq. (18), as explained previously. The result of fit *B'* is a slightly smaller value of $\langle \bar{\psi}\psi \rangle$

$$\frac{\langle \bar{\psi}\psi \rangle^{\overline{\text{MS}}}}{N_f}(2 \text{ GeV}) = -(294 (25) \text{ MeV})^3, \quad (20)$$

which is however compatible within errors with the value from Fit *B*. Also the results of fit *A'* differ only slightly from fit *A*:

$$\frac{\langle \bar{\psi}\psi \rangle^{\overline{\text{MS}}}}{N_f}(2 \text{ GeV}) = -(324 (37) \text{ MeV})^3, \quad m_q^{\overline{\text{MS}}}(2 \text{ GeV}) = 3.0 (4) \text{ MeV}. \quad (21)$$

If we had performed fit *A* (no $\langle A^2 \rangle$ term) with the same fit range, we had obtained

$$\frac{\langle \bar{\psi}\psi \rangle^{\overline{\text{MS}}}}{N_f}(2 \text{ GeV}) = -(335 (37) \text{ MeV})^3, \quad m_q^{\overline{\text{MS}}}(2 \text{ GeV}) = 3.0 (4) \text{ MeV}.$$

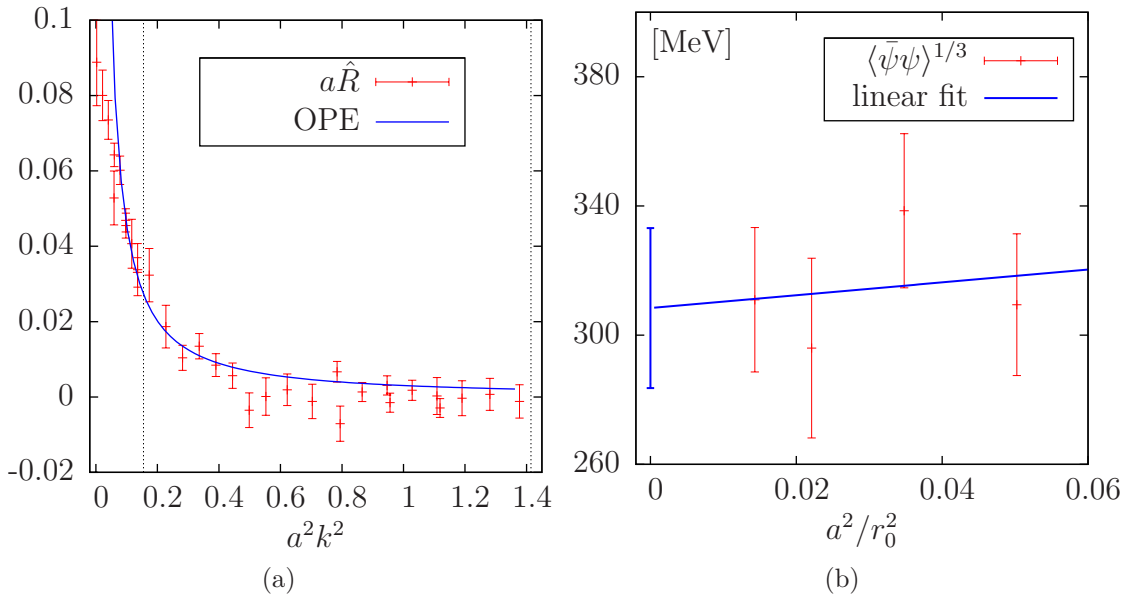


Figure 8: (left) Fit of $a\hat{R}$ in the chiral limit using fit strategy B for $\beta = 4.05$. The vertical lines indicate the fit range. (right) Continuum limit extrapolation of $\langle\bar{\psi}\psi\rangle$.

Thus, the difference is well covered by the purely statistical error which is quoted here. It is worthwhile to note that in both cases we were able to get reasonable stable fits of the fitted parameters $\langle\bar{\psi}\psi\rangle$ and m_q when including the $\langle A^2 \rangle$ term in the fit with fixed values. We conclude that although we were not able to fit both nonperturbative condensates independently we get consistent results for $\langle\bar{\psi}\psi\rangle$ and m_q with and without the contribution of $\langle A^2 \rangle$.

5.4 Fit C: Determination of the Quark and Gluon Condensates.

A drawback of the previous fitting strategies is that the sensitivity of the scalar to the vector form factor ratio, Eq. (14), to the value of the gluon condensate is quite limited. As a matter of fact the gluon condensate is either assumed to be zero (as in the fits A and B) or fixed at the value extracted from the analysis of the data for the form factor \hat{V} extrapolated to the chiral limit (as in the fits A' and B'). The main reason for such a limited sensitivity is that, by expanding the denominator in Eq. (14), the power corrections depending on $\langle A^2 \rangle$ appear always multiplied by the quark mass m_q , which is a small quantity. Moreover, the results of the previous fits suggest that the values of quark and gluon condensates are anti-correlated to each other. Therefore, in fit C we use the data for the corrected form factors \hat{S} and \hat{V} , separately, in order to determine simultaneously both condensates. The price to be paid is the introduction of the renormalization constant of the quark field, Z_q , which is treated as a free parameter for each value of the lattice spacing.

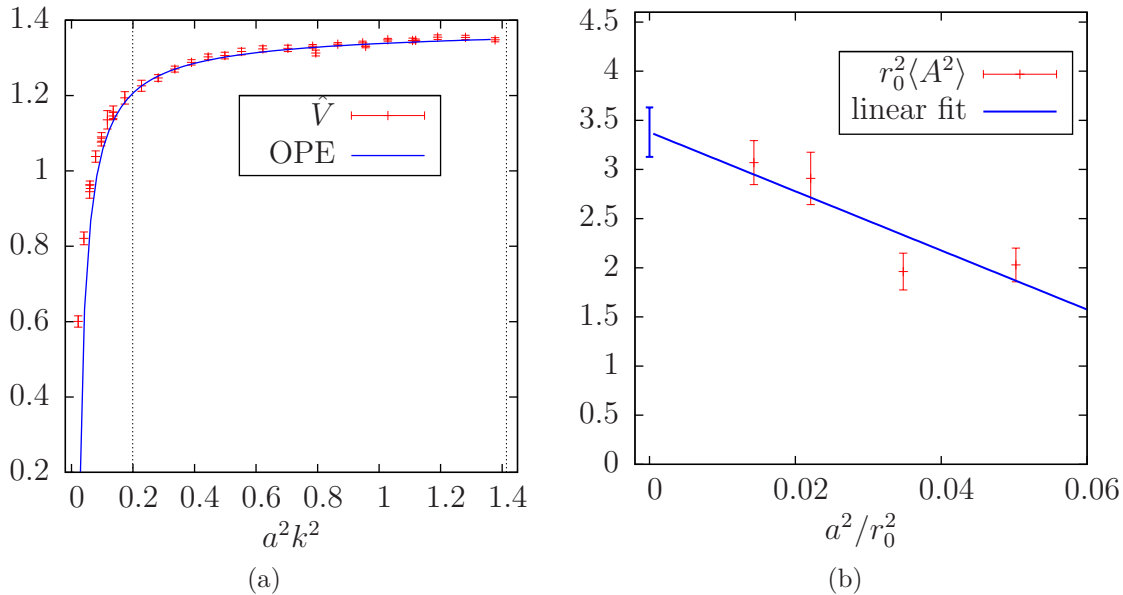


Figure 9: (left) Chirally extrapolated vector form factor \hat{V} and fits of perturbation theory to data at $\beta = 4.05$. The vertical lines indicate the fit range. (right) The continuum extrapolation of $r_0^2 \langle A^2 \rangle$ for $n_{\max} = 2$ in a^2/r_0^2 .

At the same time one of the main outcome of the previous analyses is that the discretization effects on the quark mass and on the condensates appear to be proportional to the square of the lattice spacing and, moreover, the light u/d quark mass obtained in the continuum limit and at the physical point turns out to be in good agreement with the existing estimates made by the ETMC (see Ref. [8]). Thus, we try also an alternative description of the lattice artifacts by fixing the physical quark masses m_q to their Z_P -based values and by performing in Eqs. (5) and (6) the following replacements:

$$\begin{aligned}
 m_q &\rightarrow \frac{1}{Z_P a} (a\mu_q) \cdot \left(1 + D_m \frac{a^2}{r_0^2} \right), \\
 \langle \bar{\psi}\psi \rangle &\rightarrow \langle \bar{\psi}\psi \rangle \cdot \left(1 + D_{\bar{\psi}\psi} \frac{a^2}{r_0^2} \right), \\
 \langle A^2 \rangle &\rightarrow \langle A^2 \rangle \cdot \left(1 + D_{A^2} \frac{a^2}{r_0^2} \right),
 \end{aligned}$$

where D_m , $D_{\bar{\psi}\psi}$ and D_{A^2} are free parameters (independent on the lattice spacing). Finally, two discretization terms of the form $D_{S(V)} a^2 k^2$, where $D_{S(V)}$ is a free parameter, are added to Eqs. (5) and (6), respectively, to take into account possible discretization effects proportional to the squared momentum. The impact of such terms on the extraction of the quark and gluon condensates turns out to be quite limited.

A total of 640 data points are analysed using 11 free parameters, obtaining a χ^2 per degree

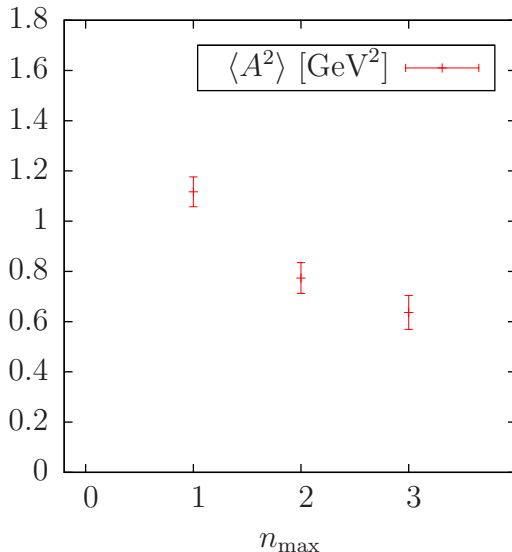


Figure 10: n_{\max} dependence of the fitted gluon condensate $\langle A^2 \rangle$ after continuum extrapolation.

of freedom of ~ 0.9 . The quark and gluon condensates turn out to be:

$$\frac{\langle \bar{\psi}\psi \rangle^{\overline{\text{MS}}}}{N_f} = -(270 (15) (20) \text{ MeV})^3,$$

$$\langle A^2 \rangle^{\overline{\text{MS}}} = 0.56 (06) (12) \text{ GeV}^2,$$

where the second error is the systematic one reflecting the uncertainty in the truncation of the perturbative series. The value obtained for $\langle A^2 \rangle$ agrees with the one used in fits A' and B' . Furthermore, our estimates for $\langle A^2 \rangle$ agree with the result $g^2 \langle A^2 \rangle_{\mu=10 \text{ GeV}}^{\overline{\text{MS}}} = 2.01 (11) \text{ }^{(+0.61)}_{(-0.73)} \text{ GeV}^2$ obtained in Ref. [31] from the analysis of the Landau gauge quark propagator as in the present paper. The latter, once evolved at the scale $\mu = 2 \text{ GeV}$, corresponds to $\langle A^2 \rangle_{\mu=2 \text{ GeV}}^{\overline{\text{MS}}} = 0.67 (04) \text{ }^{(+0.20)}_{(-0.24)} \text{ GeV}^2$.

The result for the quark condensate as obtained from fit C is a bit below the results obtained in the previous fits. This means that different treatments of the quark mass dependence of the leading term of the OPE of the quark propagator may lead to a systematic effect of $\sim 30 \text{ MeV}$ on the extracted value of the quark condensate.

Overall we conclude from the comparison of primed with non-primed fits that the contamination of nonperturbative effects in our data is inducing errors that are well covered by the uncertainties we quote.

6 Conclusions

We have presented a study of the quark propagator on the lattice using $N_f = 2$ Wilson twisted mass fermions. By comparing the numerical data to perturbative series we were

quantity	final value	fitting method
$\langle\bar{\psi}\psi\rangle/N_f$	$-(335 (37) (35) \text{ MeV})^3$	Fit <i>A</i>
m_q	3.0 (4) (2) MeV	
$\langle\bar{\psi}\psi\rangle/N_f$	$-(\mathbf{299 (26) (29) MeV})^3$	Fit <i>B</i>
$\langle\bar{\psi}\psi\rangle/N_f$	$-(324 (37) (34) \text{ MeV})^3$	
m_q	3.0 (4) (2) MeV	Fit <i>A'</i>
$\langle A^2 \rangle$	$(0.65 (09) (17) \text{ GeV})^2$	
$\langle\bar{\psi}\psi\rangle/N_f$	$-(294 (25) (28) \text{ MeV})^3$	Fit <i>B'</i>
$\langle A^2 \rangle$	$(0.65 (09) (17) \text{ GeV})^2$	
$\langle\bar{\psi}\psi\rangle/N_f$	$-(270 (15) (20) \text{ MeV})^3$	Fit <i>C</i>
$\langle A^2 \rangle$	$(0.56 (06) (12) \text{ GeV})^2$	

Table 3: Final values of our fit parameters $\langle\bar{\psi}\psi\rangle$, m_q and $\langle A^2 \rangle$, all in the $\overline{\text{MS}}$ scheme at scale $\mu = 2 \text{ GeV}$. The value m_q corresponds to the physical point, whereas $\langle\bar{\psi}\psi\rangle$ and $\langle A^2 \rangle$ are understood to be defined in the chiral limit. We emphasize that (only) the fit strategies *B* and *B'* provide an explicit extrapolation of the data to the chiral limit. This is why the *B*-fit value for $\langle\bar{\psi}\psi\rangle$ is quoted in Eq. (3).

able to determine estimates for the quark mass and the chiral condensate, which both are fundamental parameters of QCD. A summary of the results for the different analysis methods can be found in Table 3. From these results, we obtain our final estimates printed in bold font in Table 3 and quoted in Eqs. (2) and (3) and in the abstract. The results we obtain are well compatible with other lattice determinations obtained using alternative approaches, while the errors we quote appear to be larger. However, we believe that these errors give a fair estimate in particular of the systematic uncertainties involved in the kind of analysis we applied in this paper.

Therefore, we conclude that a combined perturbative and lattice analysis of the quark propagator is possible with recent lattice data, even if the errors are still large. Smaller values of the lattice spacing are desirable, since they would allow us to include larger values of the momenta in the analysis.

We have also studied nonperturbative contaminations of our results at small values of the momenta, which is in the literature often interpreted as a contribution of the gluon condensate A^2 . We do see contributions from such terms, which are, however, not stable over the order in perturbation theory. In fact, in the continuum limit the contribution decreases with increasing order in α_s , and we do not observe any saturation as is visible in Fig. 10. Still, our value for the gluon condensate is compatible with the findings reported in Ref. [31].

Acknowledgements

We would like to thank Konstantin G. Chetyrkin, Johann H. Kühn, and Karl Jansen for initiating this work and for useful discussions. We thank all members of the ETM Collaboration for the most fruitful collaboration. We thank Martha Constantinou for communicating her one-loop lattice perturbation theory results prior to publication and Benoit Blossier for discussions. This work has been supported in part by the DFG Collaborative Research Center SFB/TR9 as well as by the DFG and the NSFC through funds provided to the sino-german CRC 110. F.B. acknowledges financial support by the DFG-funded Graduate School GK 1504. V.L. and S.S. thank MIUR (Italy) for partial support under the contract PRIN08. For data generation we have used the open source tmLQCD software suite [33] and bQCD. In our analysis we have been relying on the open source statistics package R [34].

References

- [1] D. Becirevic, V. Gimenez, V. Lubicz and G. Martinelli, Phys.Rev. **D61**, 114507 (2000), [arXiv:hep-lat/9909082](#) [[hep-lat](#)].
- [2] D. Becirevic and V. Lubicz, Phys.Lett. **B600**, 83 (2004), [arXiv:hep-ph/0403044](#) [[hep-ph](#)].
- [3] V. Gimenez, V. Lubicz, F. Mescia, V. Porretti and J. Reyes, Eur.Phys.J. **C41**, 535 (2005), [arXiv:hep-lat/0503001](#) [[hep-lat](#)].
- [4] **Alpha** Collaboration, R. Frezzotti, P. A. Grassi, S. Sint and P. Weisz, JHEP **08**, 058 (2001), [arXiv:\[hep-lat/0101001\]](#).
- [5] R. Frezzotti and G. Rossi, JHEP **0408**, 007 (2004), [arXiv:hep-lat/0306014](#) [[hep-lat](#)].
- [6] M. Constantinou, V. Lubicz, H. Panagopoulos and F. Stylianou, JHEP **10**, 064 (2009), [arXiv:0907.0381](#) [[hep-lat](#)].
- [7] C. Alexandrou, M. Constantinou, T. Korzec, H. Panagopoulos and F. Stylianou, in preparation (2011).
- [8] **ETM** Collaboration, R. Baron *et al.*, JHEP **08**, 097 (2010), [arXiv:0911.5061](#) [[hep-lat](#)].
- [9] **ETM** Collaboration, P. Boucaud *et al.*, Phys. Lett. **B650**, 304 (2007), [arXiv:\[hep-lat/0701012\]](#).
- [10] **ETM** Collaboration, C. Urbach, PoS **LAT2007**, 022 (2007), [arXiv:0710.1517](#) [[hep-lat](#)].

- [11] **ETM** Collaboration, P. Boucaud *et al.*, Comput.Phys.Commun. **179**, 695 (2008), arXiv:0803.0224 [hep-lat].
- [12] K. G. Chetyrkin and A. Retey, Nucl. Phys. **B583**, 3 (2000), arXiv:[hep-ph/9910332].
- [13] K. Chetyrkin and A. Maier, JHEP **1001**, 092 (2010), arXiv:0911.0594 [hep-ph].
- [14] K. G. Chetyrkin, J. H. Kühn and M. Steinhauser, Comput. Phys. Commun. **133**, 43 (2000), arXiv:[hep-ph/0004189].
- [15] A. Shindler, Phys. Rept. **461**, 37 (2008), arXiv:[0707.4093] [hep-lat].
- [16] P. Weisz, Nucl. Phys. **B212**, 1 (1983).
- [17] R. Frezzotti and G. Rossi, JHEP **0410**, 070 (2004), arXiv:hep-lat/0407002 [hep-lat].
- [18] J. E. Mandula and M. Ogilvie, Phys. Lett. **B248**, 156 (1990).
- [19] A. Sternbeck, E.-M. Ilgenfritz, M. Müller-Preussker and A. Schiller, Phys.Rev. **D72**, 014507 (2005), arXiv:hep-lat/0506007 [hep-lat].
- [20] **ETM** Collaboration, M. Constantinou *et al.*, JHEP **1008**, 068 (2010), arXiv:1004.1115 [hep-lat].
- [21] **UKQCD** Collaboration, D. B. Leinweber, J. I. Skullerud, A. G. Williams and C. Parrinello, Phys. Rev. **D60**, 094507 (1999), arXiv:[hep-lat/9811027].
- [22] R. Sommer, Nucl. Phys. **B411**, 839 (1994), arXiv:[hep-lat/9310022].
- [23] P. Boucaud *et al.*, Phys.Rev. **D74**, 034505 (2006), arXiv:hep-lat/0504017 [hep-lat].
- [24] **ETM** Collaboration, B. Blossier *et al.*, Phys.Rev. **D82**, 034510 (2010), arXiv:1005.5290 [hep-lat].
- [25] O. Pene *et al.*, PoS **FACESQCD**, 010 (2010), arXiv:1102.1535 [hep-lat].
- [26] **ETM** Collaboration, B. Blossier *et al.*, Phys.Rev. **D82**, 114513 (2010), arXiv:1010.3659 [hep-lat].
- [27] C. Michael, Phys. Rev. **D49**, 2616 (1994), arXiv:[hep-lat/9310026].
- [28] **ETM** Collaboration, K. Jansen, F. Karbstein, A. Nagy and M. Wagner, JHEP **1201**, 025 (2012), arXiv:1110.6859 [hep-ph].
- [29] P. Fritzsche *et al.*, Nucl.Phys. **B865**, 397 (2012), arXiv:1205.5380 [hep-lat].

- [30] **Particle Data Group** Collaboration, W. M. Yao *et al.*, J. Phys. **G33**, 1 (2006).
- [31] **ETM** Collaboration, B. Blossier *et al.*, Phys.Rev. **D83**, 074506 (2011),
arXiv:1011.2414 [hep-ph].
- [32] S. Narison and V. I. Zakharov, Phys. Lett. **B679**, 355 (2009),
arXiv:0906.4312 [hep-ph].
- [33] K. Jansen and C. Urbach, Comput.Phys.Commun. **180**, 2717 (2009),
arXiv:0905.3331 [hep-lat].
- [34] R Development Core Team, *R: A language and environment for statistical computing*,
R Foundation for Statistical Computing, Vienna, Austria, 2010, ISBN 3-900051-07-0.